ELSEVIER

Infrared Physics & Technology 40 (1999) 141–151

INFRARED PHYSICS & TECHNOLOGY

www.elsevier.com/locate/infrared

Novel design concepts of widely tunable germanium terahertz lasers

E. Bründermann *, D.R. Chamberlin [1], E.E. Haller [2]

Lawrence Berkeley National Laboratory and University of California, Berkeley, CA 94720, USA

Abstract

We explore the full parameter space for laser operation and compile guidelines for building improved Ge lasers, especially for continuous wave applications. We present laser emission from p-type Ge lasers with small volumes at high repetition rates and with inter-contact distances as low as 750 μm. The emission is analyzed as a function of the current–voltage characteristic. The Poisson equation is solved to determine the electric field distribution and two new laser designs are presented.

PACS: 42.55.Px; 42.70.Hj; 78.45.+h

Keywords: Germanium; Far-infrared; Semiconductor laser; Tunable laser; Local oscillator; Heterodyne receivers

1. Introduction

Many physical phenomena have signatures in the terahertz (THz) frequency region: quantized rotational states of molecules and hyper fine structure lines of atoms [1]; van der Waals bonding energies, e.g., in soft molecule crystals and organic semiconductors; acoustical and optical phonons; hole energy states and cyclotron resonance frequencies in 3D and 2D systems. Despite the potential wealth of scientific information, studies of these phenomena have been handicapped by the lack of an easily accessible, coherent, compact, powerful and tunable source operating in the THz frequency range.

Germanium hot hole lasers emit THz radiation up to several watts in a pulsed mode (for a review see Ref. [2]). They operate with an inversion of the hole population between the light and heavy hole bands in crossed electric and magnetic fields. The light hole states represent the upper laser states. Before 1995, Ge lasers were operated with duty cycles of the order of 10^{-5}. We were able to drastically improve the performance of these lasers with the discovery of high optical gain in Be-doped Ge [3]. This material has led to duty cycles of 2.5%. Ge lasers can be operated at repetition rates up to 45 kHz [4]. The emitted laser pulse can last up to 32 μs. Our Ge:Be lasers can be tuned continuously from 1 to 4 THz [5]. They can be operated with small permanent magnets [6,7] and in closed-cycle refrigerators at temperatures of up to 20–30 K [4,6]. Single line operation and

* Corresponding author. E.O. Lawrence Berkeley Laboratory, Material Science Division, Mailstop 2-200, 1 Cyclotron Road, Berkeley, CA 94720, USA. E-mail: e_brundermann@lbl.gov.

[1] E-mail: drchamberlin@lbl.gov.

[2] E-mail: eehaller@lbl.gov.

1350-4495/99/$ - see front matter
PII: S1350-4495(99)00006-7

mode line widths of 1 MHz have been demonstrated in Ga-doped Ge lasers [8–11].

For continuous wave operation of Ge lasers, we have to reduce their power consumption and we need to increase the conversion efficiency. In this article, we focus on the electrical parameters which influence the power consumption of the Ge laser. We relate those parameters to the applied fields, to the crystal properties, to the dopant species and to the emitted stimulated emission. Traditionally, the Ge laser shape has been a rectangular parallelepiped with two opposing ohmic contacts covering two surfaces *completely*.

Our approach to reach continuous wave operation of Ge lasers is to design an active laser volume with a homogeneous field distribution while utilizing the inactive, electric field-free Ge laser material as a heat sink. Therefore, we analyze the electric field distribution throughout the Ge laser volume. We present two new ohmic contact geometries which may lead to a variety of new laser designs. Those geometries rely entirely on the use of Ge laser material doped with semi-deep acceptors (e.g., Be, Zn, Cu).

2. Experimental set-up

The method of the laser crystal preparation and the typical experimental set-ups have been described in detail [3–6,12]. For laser operation, the crystals are immersed in liquid helium (LHe) at 4.2 K. We use a superconducting coil to generate a variable, DC magnetic induction (B) up to 3 T for the Faraday configuration [3]. For the Voigt configuration, two NdFeB permanent magnets of size $20 \times 10 \times 10\ \mathrm{mm}^3$ with a remanent induction of $B_R = 1.2$ T are placed at opposite surfaces of the laser crystals separated by the crystal thickness [4,6]. No soft iron is used to close the magnetic field lines because finite element calculations did not show a significant increase in the magnetic induction. Oxygen-free high conductivity (OFHC) copper heat sinks were attached to the ohmic contacts of some of the lasers. Thin indium sheets were inserted between the contacts and the heat sinks to increase the contact area and to fill voids in the Ge–Cu joint due to surface roughness. The applied electric field was pulsed with variable pulse lengths (0.1–100 μs) and repetition rates (1 Hz–100 kHz). The polished Ge surfaces allow lasing without an external cavity because of internal reflection caused by the high refractive index of Ge. Emission pulses were measured by fast Ge:Ga photoconductors and observed on a 500 MHz digital oscilloscope. The spectral measurements presented here were made with a grating spectrometer with a low resolution of 0.5–1 cm^{-1}. The crystals studied except those with new contact geometries are listed in Table 1. The material used for the lasers with new geometries is identical to the material used for L1, L2 and L6.

Table 1
Ge crystals used in this article: acceptor species, acceptor doping concentration N_A, length L, width b, inter-contact distance d

	Acceptor	N_A (10^{14} cm^{-3})	$L \times b \times d$ (mm × mm × mm)
L0	Be	4.2	5.1 × 5.1 × 7.6
L1	Be	1.4	3.0 × 2.0 × 3.0
L2	Be	1.4	18 × 3.0 × 3.0
L3	Be	0.3	12 × 2.0 × 2.0
L4	Cu	15	7.5 × 3.0 × 2.0
L5	Al	1.2	3.0 × 2.0 × 4.0
L6	Be	1.4	10 × 2.4 × 0.75

3. Hole population inversion and field homogeneity

The formation of the hole population inversion can be described in a simplified, semi-classical picture [13]. The main trajectory of holes at 4.2 K (LHe) in crossed electric $\vec{E}$ and magnetic $\vec{B}$ fields can be approximated with an orbit in velocity space, neglecting all scattering events. The hole oscillates through the origin in an orbit centered at the drift velocity given by the applied fields $v_D = E/B$. In the energy-momentum space, this oscillation corresponds to an energy oscillation between $W = 0$ and $W = 2m^* v_D^2$ with the hole effective mass m^*. The light hole effective mass m_L^* and the heavy hole effective mass $m_H^* \approx 8 \times m_L^*$ determine different maximum energies for the light holes, $W_L = 2m_L^* v_D^2$, and for the heavy holes, $W_H = 2m_H^* v_D^2$, respectively. Heavy holes scatter into the light hole band with a probability given by the ratio of the heavy and light hole band densities of state when $W_H > W_{OP}$ where

W_{OP} denotes the optical phonon energy in Ge of 37 meV. A population inversion results when light holes do not scatter with optical phonons ($W_L < W_{OP}$). The heavy holes cannot reach the optical phonon energy ($W_H < W_{OP}$) for a field ratio smaller than 0.96 kV/(cm T). Therefore, the pumping of heavy holes into the light hole band ceases and laser emission does not occur. At field ratios higher than 2.75 kV/(cm T) ($W_L > W_{OP}$), both heavy and light holes emit optical phonons and the hole population inversion is destroyed. This model predicts that optimum pumping is achieved when the heavy hole energy W_H coincides with the optical phonon energy for a field ratio of $E/B = 0.96$ kV/(cm T) which corresponds to a drift velocity of $v_D \approx 10^5$ cm/s. For this case, the heavy hole can scatter into the light hole band with zero remaining kinetic energy.

In another description, we can evaluate the area where holes do not emit optical phonons while moving on trajectories in velocity space in relation to the whole velocity space which is defined by the inside area of a circle with a radius of v_{OP} (Fig. 1a). v_{OP} corresponds to the optical phonon energy $W_{OP} = m^* v_{OP}^2/2$. In three dimensions, the hole trajectories without optical phonon scattering occupy spindle-shaped volumes (Fig. 1b). If we denote the volume of the spindle as V^S, we can relate it to the whole volume of the sphere $V = 4\pi v_{OP}^3/3$. We find the probability for the accumulation of light holes $P_L = V_L^S/V$. The probability of heavy hole scattering P_H which defines the rate of scattering into the light hole band can be calculated as the volume V minus the heavy holes trapped in the spindle volume V_H^S as $P_H = 1 - V_H^S/V$ (Fig. 2). The product $P_L \times P_H$ shows a maximum probability for a hole population inversion at $E/B = 1$ kV/(cm T), similar to the semi-classical picture.

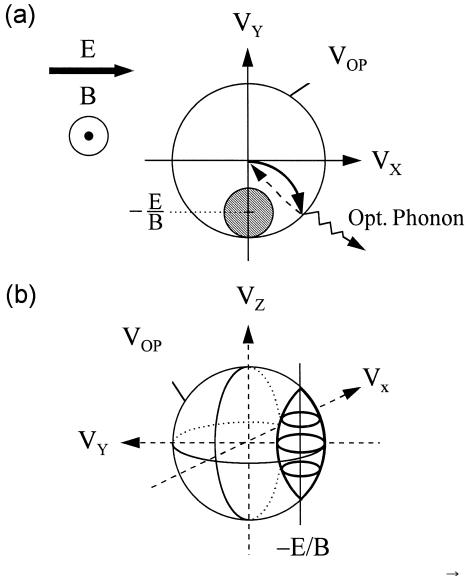

Fig. 1. (a) Two dimensional velocity space in crossed $\vec{E}$ and $\vec{B}$ fields. The main hole trajectories start at the origin. Oblique hatching: trajectories of holes with a long lifetime, holes do not emit optical phonons. (b) Trajectories of holes without optical phonon scattering in three dimensions form a spindle-shaped volume.

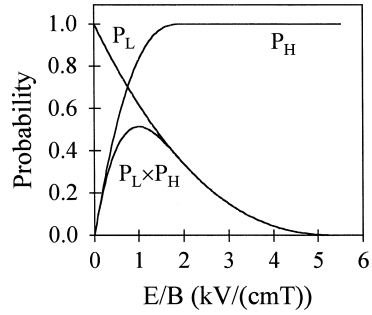

Fig. 2. Probability of light hole accumulation P_L and heavy hole scattering with optical phonons P_H vs. the field strength ratio E/B. The product $P_L \times P_H$ describes the probability for inversion formation in Ge.

For optimal laser amplification, the ratio E/B should be kept constant in the whole active laser volume, especially if a resonant model is considered where the heavy hole energy precisely reaches the optical phonon energy ($W_H = W_{OP}$). Such resonances have been observed experimentally for first order and higher order resonances where the maximum heavy hole energy coincides with two, three or more optical phonons $W_H = nW_{OP}$ ($n = 2, 3, \ldots$) [4,13].

Stoklitskiy [14] calculated the lifetime of holes in light hole Landau levels at a magnetic induction B parallel to the crystallographic orientation ⟨110⟩ for different electric field orientations in the (110) plane. He showed that the longest lifetime can be achieved with the electric field pointing parallel to another ⟨110⟩ direction. Varying the field orientation in the (110) plane can reduce the light hole lifetime by

several orders of magnitude. Therefore, a constant electric field orientation has to be achieved throughout the active laser volume.

The laser mechanism crucially depends on orthogonal electric and magnetic fields. An electric field component parallel to the magnetic field leads to an acceleration of the holes in the direction of the magnetic field. They quickly reach the optical phonon energy and emit optical phonons so that the lifetime of the light holes is significantly reduced. This effect was used for the development of mode-locked Ge lasers [15]. Additional electrical contacts were used to intentionally apply a modulated electric field parallel to the magnetic field.

At a constant applied electric field, magnetic field inhomogeniety leads to emissions over a range of frequencies (Fig. 3). The laser emission frequency depends on the magnetic field due to the energy dependence of the light hole Landau levels which are the upper laser states. They are spaced with the cyclotron resonance energy $h\nu = \hbar eB/m_{\mathrm{L}}^{*}$. The corresponding frequency ν changes by 20.3 $\mathrm{cm}^{-1}/\mathrm{T}$ as indicated by the dashed line in Fig. 3. We find that the maximum emission occurs at $E/B \approx 1$ kV/(cm T) at $\nu \approx 80$ cm^{-1}. The emission could be related to a transition from a light hole Landau level $(n+4)$ to a light hole Landau level n or to a heavy hole Landau level. An accurate assignment requires a complete quantum mechanical treatment [5,16].

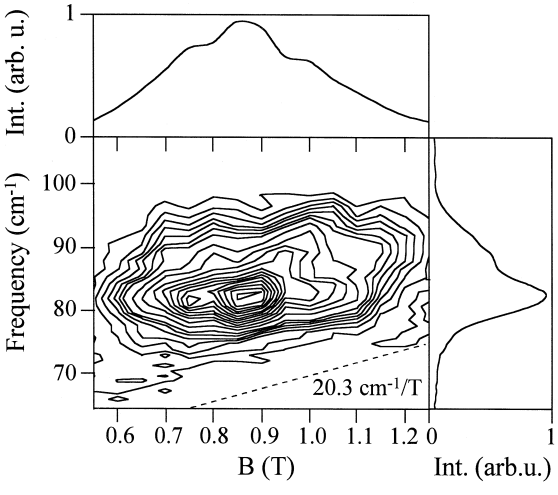

Fig. 3. Isointensity lines of the emission of laser L0 vs. magnetic induction B and vs. frequency. The applied electric field was $E = 0.83$ kV/cm. The magnetic field was provided by a superconducting coil.

At a constant magnetic field, variation of the applied electric field changes the degree of Landau level mixing as we have shown previously [5]. As a result, different lower laser levels dominate the transition frequencies in dependence of the electric field and the laser emission varies over a range of frequencies as the electric field is varied.

Stoklitskiy's calculation of the light hole lifetime dependence on the electric field orientation gives an additional argument. While changing one of the parameters E or B while leaving the other parameter constant, we change the Hall field component of the electric field in the crystal. Therefore, the total electric field which is the sum of the applied and the Hall electric field changes both orientation and strength [17].

So far we can conclude: (1) the magnetic induction B and the electric field E have to be *simultaneously* homogeneous and properly orientated in respect to the crystallographic axes throughout the lasing volume to allow optimal amplification of the desired frequencies, (2) the E/B ratio has to be constant and preferably equal to 1 kV/(cm T) throughout the lasing volume to allow an optimal formation of the hole inversion.

A homogeneous magnetic field can be generated by well-designed superconducting magnet coils or permanent magnets. However, the electric field is a complicated function of the crystal geometry, the electrical contact geometry and the Hall field component induced by the magnetic field. Recently, the electric field distribution for Ge lasers with rectangular cross-sections has been investigated theoretically by solving the Poisson equation in two dimensions [17]. Indeed, the resulting electric field strength as well as the orientation for the commonly used rectangular parallelepiped crystal geometry with a near-square cross-section is very inhomogeneous. We find the highest optical gain for a specific frequency for a homogeneously doped Ge laser only in a fraction of the crystal volume [17]. One experimental attempt was made by Bespalov and Renk [18] to improve the electric field homogeneity. They used a rhombic cross-section which was inclined by the Hall angle to improve the homogeneity of the electric field distribution due to parallel equipotential lines. They found

that the cyclotron resonance line width of the Ge laser was narrower than that of a rectangular cross-sections which they related to the improved electric field strength.

Early research focused on rather large Ge lasers with volumes of 1–2 cm^3 which were doped with shallow acceptors, mainly gallium [2]. Ge:Ga lasers are dominated by internal self-absorption by those shallow acceptors [19,20]. Be-doped Ge laser material [3] improves the laser operation by eliminating self-absorption [5]. In Zn- and Cu-doped Ge lasers, those absorptions are also eliminated [3,5,12]. Contrary to the other acceptors, Cu doping can be achieved by diffusion into pure Ge at modest temperatures and times [12,21]. We believe that the performance of a Ge laser doped with deep acceptors will be substantially improved through higher field homogeneity.

4. Continuous wave operation and electrical parameters

The laser operating temperature of 20–30 K requires a thermal power dissipation in liquid helium or in a closed cycle refrigerator around 10–20 W.

We have investigated several possibilities to achieve a reduction of the power consumption which may lead to laser operation in thermal equilibrium at the desired crystal temperatures. We have reduced the crystal volume V down to 0.5 mm^3. The power consumption P was reduced to 4 W but the emission intensity was weak [4]. The laser operated only in a pulsed mode which suggests that the coupling to the heat sinks was not optimal. In a pulsed mode, electric pulses of length t with a repetition frequency f are applied. The duty cycle DC is given by $t \times f$. The power consumption which leads to the heating of the Ge crystal lattice is then given by the mean applied power $\overline{P} = P \times \mathrm{DC}$.

There are two ways to reduce the crystal volume: first, the ohmic contact area A can be reduced which leads to a lower current I through the device; secondly, we can reduce the inter-contact distance d which lowers the applied voltage U. As a consequence, the electric field $E = U/d$ and the current density $j = I/A$ are unchanged. In addition, we can lower the acceptor doping concentration N_A to reduce the current density and therefore the current. The current density is governed by the equations:

$$j = \sigma E = eN_A\,\mu E = \frac{e^2}{m^*} N_A \tau E \qquad (1)$$

with the conductivity σ given by the mobility μ and the electron charge e. The mobility μ can be further separated by the introduction of the effective hole mass m^* and the scattering time τ. Heavy holes are the main constituent of the current due to their heavier mass and therefore higher scattering probability with optical phonons in crossed electric and magnetic fields so that m^* can be approximated with m^*_H.

If we return to the semi-classical description of heavy hole trajectories which begin at the origin of velocity space, we find that by increasing the field ratio E/B we have the on-set of optical phonon scattering at $W_H = W_{OP}$. However, this is only a sharp on-set if we disregard the distribution of the heavy holes around the main trajectory through the origin. We can assume a distribution around the main trajectory because impurity scattering and acoustical phonon scattering can redistribute the holes in velocity space below the optical phonon energy. This effect is visible in Monte Carlo simulations [22]. For $W_H > W_{OP}$, we find that the heavy holes will form a beam-like structure around the main trajectory with frequent optical phonon emissions [22,23]. If we consider a spread of trajectories for heavy holes around the main trajectory, we find that the scattering time τ will first increase with increasing field ratio E/B while the spread trajectories lead to optical phonon scattering despite $W_H < W_{OP}$. We find a maximum scattering time τ when the main trajectory with the densest population of heavy holes reaches the optical phonon energy at $W_H = W_{OP}$. A further increase of the E/B ratio, which means that the effect of the magnetic field diminishes, leads to the known saturation of the drift velocity and the scattering time. Any further electric field increase reduces the scattering time. The conductivity σ which is independent of the crystal volume and is proportional to the scattering time, is therefore a good parameter to define the optimal laser condition at $W_H = W_{OP}$. Here, σ will have a maximum and the current trace in the I–(E/B) or for a constant

induction B in the I–E-curve, will have the steepest slope.

Fig. 4a displays the laser emission of L1 as a function of the E/B ratio for different constant magnetic induction B while varying the electric field. We measured the maximum emission and the steepest slope of the I–(E/B)-curve always at $E/B = 0.96$ kV/(cm T) while the current value is unchanged. If we compare the current for different magnetic fields at the same E/B ratio for $E/B >$ 0.96 kV/(cm T), we observe a minor increase in the current value for an increasing magnetic induction. We attribute this to the incomplete ionization of the Be-acceptors [3,13]. The degree of ionization is even lower in Cu-doped Ge lasers [12]. For a constant E/B ratio, higher electric fields are necessary for a higher magnetic induction which eases ionization of the deeper Be-acceptors increasing the number of free holes which is expressed in Eq. (1) by N_A.

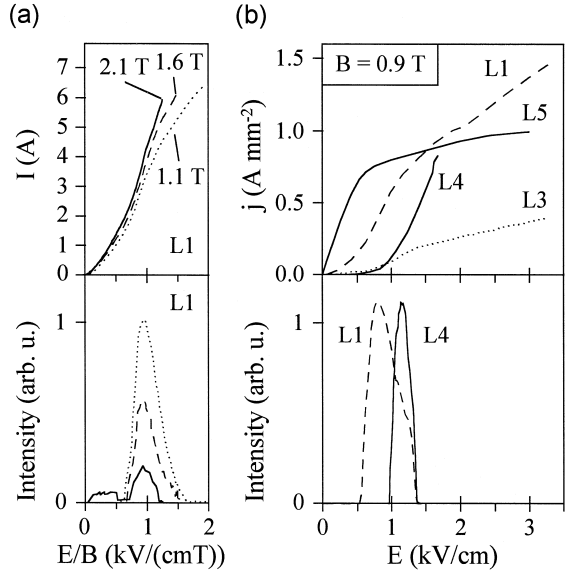

Fig. 4. (a) Laser emission intensity and current I of L1 vs. the field strength ratio E/B for different magnetic induction $B = 1.1$ T (dotted line), 1.6 T (dashed line), and 2.1 T (solid line), respectively. The electric pulse was applied for $t = 15$ μs at a repetition frequency of $f = 10$ Hz. The magnetic induction B was delivered by a superconducting magnet. (b) Current density j and laser intensity for Ge crystals with different dopant species as listed in Table 1: L1, Ge:Be laser (dashed line); L3, Ge:Be laser (dotted line); L4, Ge:Cu laser (solid line); L5, Ge:Al laser (solid line).

Fig. 4b displays the current density j and the laser intensity as a function of the electric field E for differently doped Ge crystals at the same magnetic induction of $B = 0.9$ T. The shape of the j–E-curve depends on the dopant species. We can explain the behavior of the current density for the different dopant species by a semi-classical description. The heavy hole trajectories, mainly originating in the center of the velocity space, can reach a maximum kinetic energy W_H. If this energy is below the binding energy of the acceptor, we cannot expect impact ionization. The ionization energies of Al, Be, and Cu are 11, 25 and 43 meV, respectively. For $B = 0.9$ T, we expect a rapid on-set of the current density due to impurity scattering and subsequent optical phonon scattering which increases the number of free holes N_A at $E = 0.49$, 0.78 and 0.97 kV/cm, respectively. We observe a current density also at lower electric fields for Al- and Be-doped Ge. We attribute this to resonances of the heavy holes at the kinetic energy W_H with hole transitions from the acceptor ground state to bound excited states [3]. Subsequent ionization and scattering leads to the current flow and current density. The lowest resonance energy corresponds to the G absorption line of the impurity. If we disregard the magnetic and electric field splitting of those lines, we can calculate a heavy hole kinetic energy W_H resonance with the G-line at 6.6, 20 and 39 meV, which for $B = 0.9$ T corresponds to $E =$ 0.40 kV/cm, 0.70 and 0.98 kV/cm, respectively.

The incomplete ionization of Cu-doped Ge lasers is reflected in the current density [12]. For $E < 1$ kV/cm, the free holes and the current density in L4 are similar to a 50 times lower doped Ge:Be crystal L3. The number of free holes is too small to allow laser emission which begins for L4 and L3 at $E = 1$ kV/cm. At $E = 1.5$ kV/cm, the current density of L4 is comparable to the value of the 10 times lower doped Ge:Be crystal L1. However, at $B = 0.9$ T, we significantly deviate from the optimal condition for the hole inversion $E/B = 0.96$ kV/(cm T) and lasing stops. Shallow acceptor doped Ge lasers like L5 typically emit laser radiation for $E/B \gg 1$ kV/(cm T) which is not due to the absence of sufficient-free holes during laser operation but a result of self-absorption by the shallow impurities [24,25].

We find that Be-doped Ge material with a doping concentration of $N_A = 10^{14}$ cm^{-3} allows optimal

laser emission at the optimal field ratio $E/B = 0.96$ kV/(cm T). In addition, lasers of this material can be operated at a lower field ratio E/B and subsequently lower electric field values E and lower current densities j in comparison to other dopant species in Ge. That is especially important for continuous wave emission which requires a low input power $P = jEV$.

The laser field inside the Ge crystal leads to stimulated transitions of light holes which are accumulated in the spindle volume (Fig. 1b) into the heavy hole band. Those transitions lead to an increase in the number of free heavy holes which scatter by optical phonon emission. Subsequently, a current enhancement is measured even though the pulse generator is a constant voltage source during the applied voltage pulse (Fig. 5). This enhancement can reach up to 8% for Be-doped Ge lasers while a maximum of 4% has been found for Ga- and Al-doped Ge lasers [22]. The reduction of self-absorption in Be-doped Ge lasers leads to a more efficient accumulation of light holes compared to shallow acceptor doped lasers. Subsequently, the depletion of the trapped and accumulated light holes by stimulated emission will lead to a larger current enhancement.

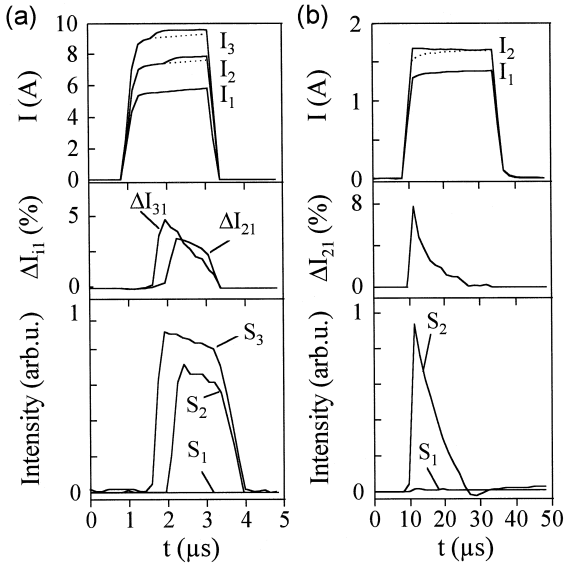

Fig. 5. (a) Emission intensity S_1, S_2 and S_3, corresponding current pulses I_1, I_2 and I_3, and current enhancements $\Delta I_{i1} = (I_i - s_i \times I_1)/(s_i \times I_1)$ for $i = 2,3$ of laser L2 at electric fields $E = 0.69$, 0.72 and 0.74 kV/cm, respectively. s is a scaling factor. The magnetic induction was $B = 0.7$ T using permanent magnets. (b) Emission intensity S_1 and S_2, corresponding current pulses I_1 and I_2, and current enhancement $\Delta I_{21} = (I_2 - s \times I_1)/(s \times I_1)$ of laser L1 at applied electric fields $E = 0.48$ and 0.52 kV/cm, respectively. The magnetic induction was $B = 0.66$ T using a superconducting magnet. The dotted lines indicate the current pulse shapes without stimulated emission.

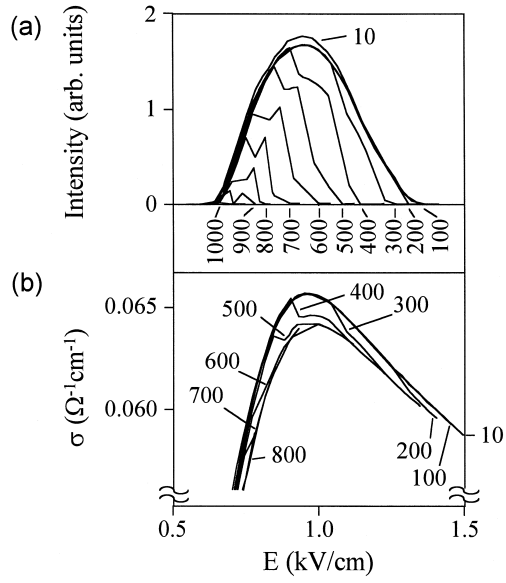

Fig. 6. (a) Laser intensity of L1 vs. electric field E and vs. repetition frequency f which ranges from 10 to 1000 Hz. The electric pulse was applied for $t = 10$ μs. (b) Conductivity σ of L1 during laser operation vs. E and f. The magnetic induction was $B = 0.9$ T using permanent magnets.

Fig. 6 shows the laser emission and the conductivity σ of L1 which changes depending on the pulse repetition rate f. As described in the semi-classical model, we find the maximum laser emission occurs at $E/B = 0.96$ kV/(cm T) where the maximum conductivity σ is found. We observe that the current enhancement (cf. Fig. 5) is also visible in the conductivity (Fig. 6b) and follows the laser intensity (Fig. 6a). The current enhancement is an independent way to measure the laser emission pulse which is typically detected by the Ge photoconductor.

Fig. 7 shows the laser emission of L1 as a function of the mean applied power $\overline{P}$ and repetition frequency f. The maximum intensity drops between 10 and 100 Hz, then remains constant up to 400 Hz. This indicates that a stable laser emission intensity

for a range of average crystal temperatures can be achieved. After each applied pulse, the laser crystal cools down until the next pulse is applied. With increasing repetition frequency, the crystal can no longer cool down completely to the LHe bath temperature and is newly pulsed at a temperature $T_{Ge} > T_{LHe} = 4.2$ K. While T_{Ge} increases with f, we find that the initial strong temperature dependence of the Ge heat capacity below 10 K leads to a rapid crystal temperature increase with the mean input power. Above 10 K, this increase slows down resulting in a constant maximum laser intensity. A further increase of the mean applied power $\overline{P} > 4$ W for $f > 400$ Hz raises the crystal temperature to a value where acoustical phonon emission becomes significant by reducing the lifetime of the accumulated light holes. A more detailed description of the thermal properties of Ge lasers using heat sinks and small dimensions has been given elsewhere [4].

Thin layer lasers with large ohmic contact areas allow optimal cooling by forming a good thermal contact to the Cu heat sinks. One step in this direction is the investigation of the minimum thickness for the inter-contact distance. Our current result is $d = 750$ μm. Fig. 8 shows the laser emission of L6 which is slightly stronger than the spontaneous emission. In addition, lasers with a short Hall geometry $d/L = 0.075$ have a homogeneous electric field strength and orientation while the Hall field has a minor influence.

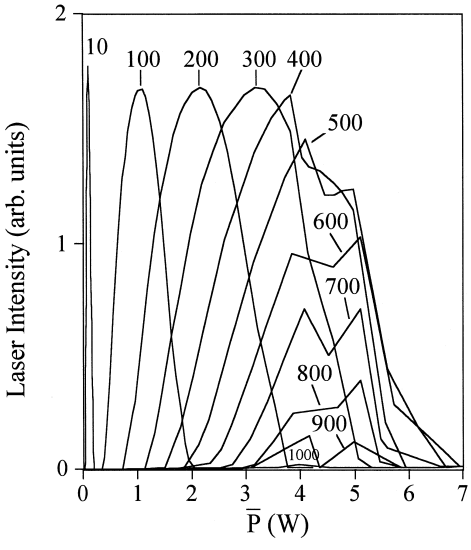

Fig. 7. Laser intensity of L1 vs. average input power $\overline{P}$ and vs. repetition frequency f which ranges from 10 to 1000 Hz. The magnetic induction was $B = 0.9$ T using permanent magnets.

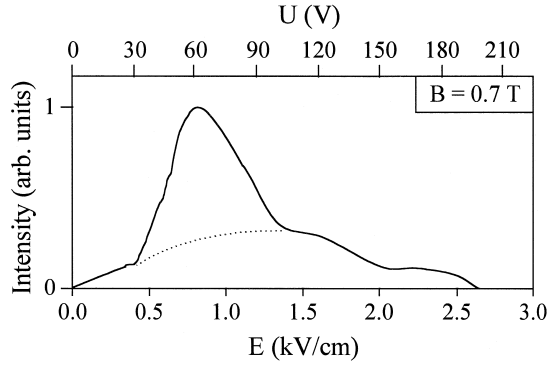

Fig. 8. Laser emission of L6 for a small inter-contact distance of 0.75 mm which is only 30 times larger than the emission wavelength inside and 7.5 times larger than outside of the Ge crystal for the magnetic induction of $B = 0.7$ T using permanent magnets. The dashed line indicates the estimated laser threshold.

5. New crystal and ohmic contact geometries

We have studied two new Ge:Be crystals and contact geometries. One is a planar device prototype with two contacts on the same surface of the laser crystal (Fig. 9a). We solved the Poisson equation for this geometry:

$$\Delta\Phi = 0 \tag{2}$$

with a finite difference technique considering the boundary conditions for those geometries in two or three dimensions [26]. The space charge was assumed to be zero. The two ohmic contacts were fixed at potentials Φ_1 and Φ_0. The other metal-free crystal surfaces have to comply with tangential current flow and the boundary conditions set by the Hall effect. With the vector $\vec{n}$ normal to the crystal surface, the current condition can be introduced by:

$$\vec{I} \cdot \vec{n} = 0. \tag{3}$$

For a magnetic field in the z direction, the Hall effect leads to a relation for the electric field components in the x and y direction. $E_x = \partial\Phi/\partial x$ and

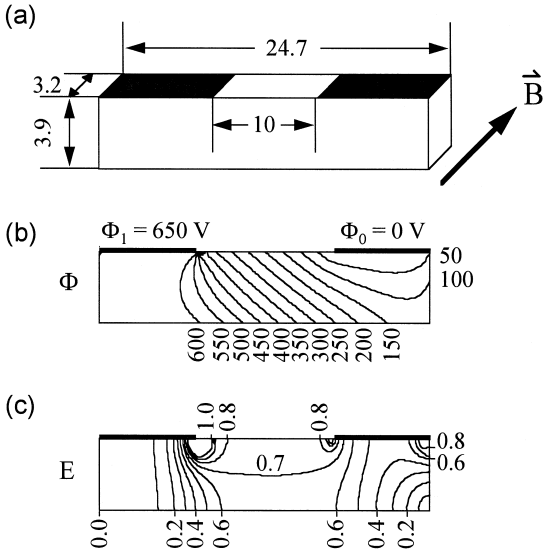

Fig. 9. (a) Study of a Be-doped Ge crystal with two ohmic contacts on the *same* surface separated by $d = 10$ mm. The magnetic induction was $B = 0.7$ T using permanent magnets. (b) Calculated potential Φ for a potential difference of $\Phi_1 - \Phi_0 = 650$ V between the ohmic contacts. The equipotential lines are indicated with 50 V spacing. (c) Calculated field lines for constant electric fields E with 0.1 kV/cm spacing.

$E_y = \partial\Phi/\partial y$ are then a function F of the tangents of the Hall angle α_H:

$$\frac{E_y}{E_x} = F\big(\tan(\alpha_H)\big). \tag{4}$$

In the calculation, the maximum Hall angle given by $\tan(\alpha_H) = \pi/2$ was used which occurs for $E/B = 0.96$ kV/(cm T) [23].

The calculation shows a very homogeneous potential distribution (Fig. 9b) between the ohmic contacts which results in a nearly constant electric field strength (Fig. 9c). The finite mesh used in this calculations allows to evaluate the electric field strength in the crystal volume by counting the occurrence of the electric field strength in 0.1 kV/cm intervals. This calculation in relation to the total number of mesh points is shown in Fig. 10a for $U = \Phi_1 - \Phi_0 = 650$ V. The dominant electric field strength is found to be close to $U/d = 0.65$ kV/cm. Laser emission of this crystal was detected perpendicular to the magnetic field emitted from the 3.2×3.9 mm^2 surface. It is displayed in dependence of the applied potential difference (Fig. 10b).

Fig. 11 shows another laser geometry with a volume of $18 \times 4 \times 4.1$ mm^3. One contact was reduced to 4×4 mm^2 of the opposing contact area which was 18×4 mm^2 with an inter-contact distance of 4.1 mm. The contact structure can be viewed as inverted to the geometry displayed in Fig. 9a. We calculated the potential (Fig. 11a) and the electric field distribution (Fig. 11b) and evaluated the electric field strength (Fig. 11c) in the laser volume. Laser emission was detected in the direction of the magnetic field as shown in Fig. 11d. Although the field strength is highly inhomogeneous, lasing is observed. Most of the laser volume has low electric fields and serves as a heat sink.

The successful operation of the above described laser structures rely on the use of Ge laser material with deep acceptors. Laser photons are not absorbed in those impurities so that crystal volumes without electric fields can be considered as pure Ge substrates. This new concept in Ge laser engineering may lead to a variety of new laser designs. It is possible to integrate optical resonators on the same crystal. The inherent self-absorption in shallow acceptor doped Ge lasers requires that the laser crystal

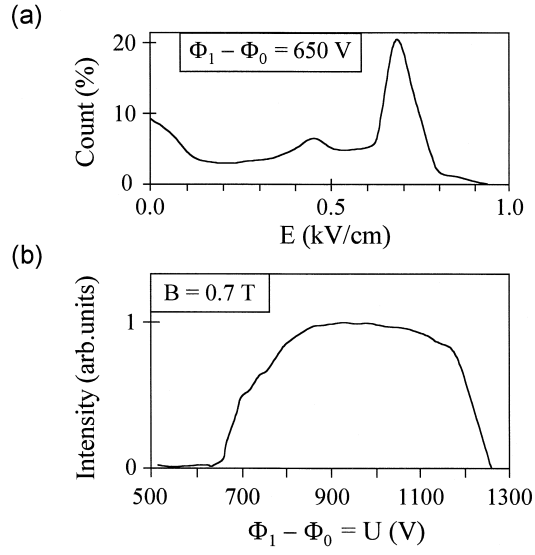

Fig. 10. (a) Count of the calculated electric fields in the Ge crystal as shown in Fig. 9a for $\Phi_1 - \Phi_0 = 650$ V. (b) Measured laser intensity of the crystal shown in Fig. 9a vs. the applied potential difference or voltage $U = \Phi_1 - \Phi_0$.

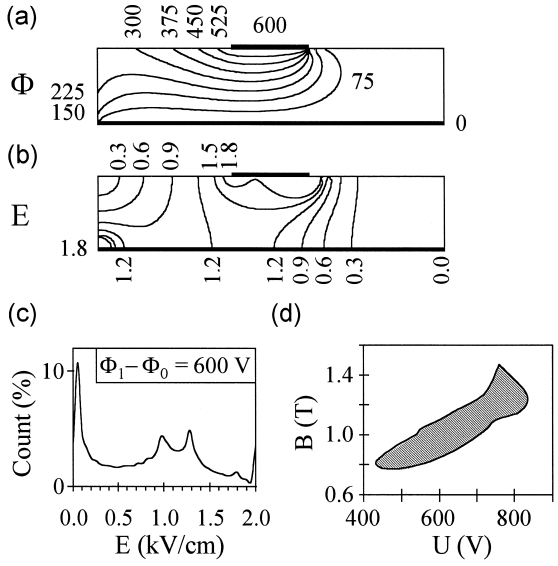

Fig. 11. Study of a Be-doped Ge crystal with an inverted contact geometry in comparison to the laser shown in Fig. 9a. The magnetic field was applied by a superconducting magnet. (a) Calculated potential Φ for a potential difference of $\Phi_1 - \Phi_0 = 600$ V between the contacts. The equipotential lines are indicated with 75 V spacing. (b) Calculated field lines for constant electric fields E with 0.3 kV/cm spacing. (c) Count of the calculated electric fields in the Ge volume. (d) Parameters in the $U-B$ plane for which laser emission was measured.

is active in the full crystal volume, meaning that electric contacts typically cover two opposite crystal surfaces *completely*. Optical resonators, typically structured metal layers, have therefore been suspended from the laser crystal by pure Si, Ge or quartz substrates to avoid electrical shorts and field disturbances [8–11]. An integration of those resonators without interfaces which are between the traditionally used substrates and the active laser medium reduces the possibility of unwanted reflections. In addition, the cooling can be improved by coupling the heat sink without interfaces to the active laser medium. Here, the heat sink is the inactive Ge.

6. Conclusion

We have derived the optimal laser parameters for Ge lasers. The optimal laser material seems to be Be-doped Ge with a Be concentration of $N_A \approx 10^{14}$ cm^{-3} operated at $E/B \approx 1$ kV/(cm T). We have demonstrated and calculated new laser geometries of Ge:Be lasers. The use of Ge laser crystals doped with semi-deep acceptors opens new possibilities for Ge laser engineering. Integrating resonators and developing new electrical contact geometries for Ge lasers offer new challenges. Inactive Ge can serve as a heat sink in which heat generated in the active parts can be dissipated. The new designs have to pay special attention to the electric field orientation and field strength. With the successful operation of the planar ohmic contact design and with possible thin active laser layers, we believe that a continuous wave Ge THz laser with a strong THz emission can be built in the near future.

Acknowledgements

We like to thank B. Tang for the preparation of Ge crystals. Partial support was provided by DLR, NE–WS, Berlin. The authors acknowledge the use of facilities at the Lawrence Berkeley National Laboratory operated under US Department of Energy Contract No. DE-AC03-76SF00098. DRC acknowledges the support of the NASA Office of Space Science Fellowship No. S98-GSRP-049. One of the authors, EB, acknowledges support by the Alexander-von-Humboldt Foundation through a Feodor-Lynen Fellowship and by the Center for Particle Astrophysics. He also thanks M.F. Kimmitt for numerous valuable comments and discussions.

References

[1] H.P. Röser, Infrared Phys. 32 (1991) 385–407.
[2] E. Gornik, A.A. Andronov (Eds.), Opt. Quantum Electron., Vol. 23 (1991) pp. S111–S360.
[3] E. Bründermann, A.M. Linhart, L.A. Reichertz, H.P. Röser, O.D. Dubon, G. Sirmain, W.L. Hansen, E.E. Haller, Appl. Phys. Lett. 68 (1996) 3075–3077.
[4] E. Bründermann, D.C. Chamberlin, E.E. Haller, Appl. Phys. Lett. 73 (1998) 2757–2759.
[5] L.A. Reichertz, O.D. Dubon, G. Sirmain, E. Bründermann, W.L. Hansen, D.R. Chamberlin, A.M. Linhart, H.P. Röser, E.E. Haller, Phys. Rev. B 56 (1997) 12069–12072.
[6] E. Bründermann, H.P. Röser, Infrared Phys. Technol. 38 (1997) 201–203.

[7] K. Park, R.E. Peale, H. Weidner, J.J. Kim, IEEE J. Quantum Electron. 32 (1996) 1203–1210.
[8] K. Unterrainer, M. Nithisoontorn, M. Helm, E. Gornik, E.E. Haller, Infrared Phys. 29 (1989) 357–360.
[9] S. Kuroda, S. Komiyama, Infrared Phys. 29 (1989) 361–369.
[10] S. Komiyama, H. Morita, I. Hosako, Jpn. J. Appl. Phys. 32 (1993) 4987–4991.
[11] E. Bründermann, H.P. Röser, A.V. Muravjov, S.G. Pavlov, V.N. Shastin, Infrared Phys. Technol. 1 (1995) 59–69.
[12] G. Sirmain, L.A. Reichertz, O.D. Dubon, E.E. Haller, W.L. Hansen, E. Bründermann, A.M. Linhart, H.P. Röser, Appl. Phys. Lett. 70 (1997) 1659–1661.
[13] E. Bründermann, A.M. Linhart, L.A. Reichertz, H.P. Röser, O.D. Dubon, W.L. Hansen, G.C. Sirmain, E.E. Haller, Proc. 23rd Int. Conf. on Physics of Semicond., 1996, pp. 3179–3182.
[14] S.A. Stoklitskiy, Semicond. Sci. Technol. 7 (1992) B610–B617.
[15] J.N. Hovenier, A.V. Muravjov, S.G. Pavlov, V.N. Shastin, R.C. Strijbos, W.Th. Wenckebach, Appl. Phys. Lett. 71 (1997) 443–445.
[16] P. Pfeffer, W. Zawadzki, K. Unterrainer, C. Kremser, C. Wurzer, E. Gornik, B. Murdin, C.R. Pidgeon, Phys. Rev. B 47 (1993) 4522–4531.
[17] R.C. Strijbos, J.E. Dijkstra, S.I. Schets, J.G.S. Lok, W.Th. Wenckebach, Semicond. Sci. Technol. 9 (1994) 648–650.
[18] A.V. Bespalov, K.F. Renk, Semicond. Sci. Technol. 9 (1994) 645–647.
[19] S.V. Demihovsky, A.V. Muravjov, S.G. Pavlov, V.N. Shastin, Semicond. Sci. Technol. 7 (1992) B622–B625.
[20] W. Heiss, K. Unterrainer, E. Gornik, W.L. Hansen, E.E. Haller, Semicond. Sci. Technol. 9 (1994) B638–B640.
[21] H. Bracht, N.A. Stolwijk, H. Mehrer, Phys. Rev. B 18 (1991) 14465–14477.
[22] A.A. Andronov, Yu.N. Nozdrin, V.N. Shastin, Infrared Phys. 27 (1987) 31–38.
[23] S. Komiyama, T. Masumi, K. Kajita, Phys. Rev. B 20 (1979) 5192–5216.
[24] E. Bründermann, H.P. Röser, W. Heiss, E. Gornik, E.E. Haller, Appl. Phys. Lett. 67 (1995) 3543–3545.
[25] E. Bründermann, A.M. Linhart, H.P. Röser, O.D. Dubon, W.L. Hansen, E.E. Haller, Appl. Phys. Lett. 68 (1996) 1359–1361.
[26] G.H. Shortley, R. Weller, J. Appl. Phys. 9 (1938) 338–348.